Numerical simulation of blood flows in human aorta

Hiroshi Suito, Viet Q. H. Huynh

Advanced Institute for Materials Research, Tohoku University

Koki Otera

Graduate School of Environmental and Life Sciences, Okayama University

Naohiro Horio

Department of Cardiovascular Surgery, Okayama University Hospital

1 Introduction

In recent years, congenital diseases such as hypoplastic left heart syndrome constitute an important issue for our society. For these and other diseases related to blood flows, fluid dynamics can be useful to elucidate the mechanisms of targeted diseases. Differences in the vessel morphology can produce different flow characteristics, stress distributions, and ultimately different outcomes. Therefore, the characterization of the morphologies of these vessels poses an important clinical question. In this paper, an example from hypoplastic left heart syndrome illustrating relations between geometrical characteristics of blood vessels and flow structures is discussed.

2 Numerical method

We adopted incompressible Navier–Stokes equations as governing equations.

$$
\begin{cases}
\frac{\partial u_i}{\partial t} + u_j \frac{\partial u_i}{\partial x_j} = -\frac{1}{\rho}\frac{\partial p}{\partial x_i} + \nu \frac{\partial}{\partial x_j}\left(\frac{\partial u_i}{\partial x_j} + \frac{\partial u_j}{\partial x_i}\right) & \text{in } \Omega \times (0,T) \\
\frac{\partial u_j}{\partial x_j} = 0
\end{cases}
\tag{1}
$$

where $t, u_i\ (i = 1, 2, 3)$, p, ρ, and ν respectively represent time, velocity, pressure, density, and the kinematic viscosity of blood. We assumed that blood can be regarded as a Newtonian fluid in large arteries. We also assumed the blood vessel as a rigid body. We utilized finite element formulation with the streamline-upwind/Petrov-Galerkin (SUPG) and pressure-stabilizing/Petrov-Galerkin (PSPG) methods to solve the problem numerically.

3 A patient-specific simulation

Our target is the geometry around an anastomosis site of aortic arch and pulmonary artery after Norwood surgery, which is one step taken during surgeries for hypoplastic left heart syndrome. Geometry of the target is extracted from a CT-Scan with boundary conditions obtained from ultrasound measurements.

Figure 1(a) and (b) portray the boundaries in our model; Γ_1 represents the vessel wall; Γ_2 denotes the cross-section of the pulmonary artery which is the inflow boundary in our model; Γ_3 is the original ascending aorta but the flow rate is very small because of the congenital disease; Γ_4, Γ_5, and Γ_6 respectively represent the brachiocephalic trunk, left carotid artery, and left subclavian artery; Γ_7 is the outflow boundary which follows down to the abdominal aorta. The vessel wall Γ_1 is assumed to be rigid. On

$\Gamma_i (i = 2, 3, 4, 5, 6)$, the velocity profiles obtained from ultrasound measurements are given as Dirichlet boundary conditions. We present zero-traction on Γ_7 to be a free outflow boundary.

$$\begin{cases} u_i = 0 & \text{on } \Gamma_1 \times (0, T), (i = 1, 2, 3), \\ u_i = v_i^j & \text{on } \Gamma_j \times (0, T), (i = 1, 2, 3)(j = 2, 3, 4, 5, 6), \\ \sigma_i = 0 & \text{on } \Gamma_7 \times (0, T), (i = 1, 2, 3), \end{cases} \tag{2}$$

where v_i^j are ultrasound measurement data shown in Fig. 2.

(a) Boundaries (front view)   (b) Boundaries (side view)   (c) Cross-section on aortic arch
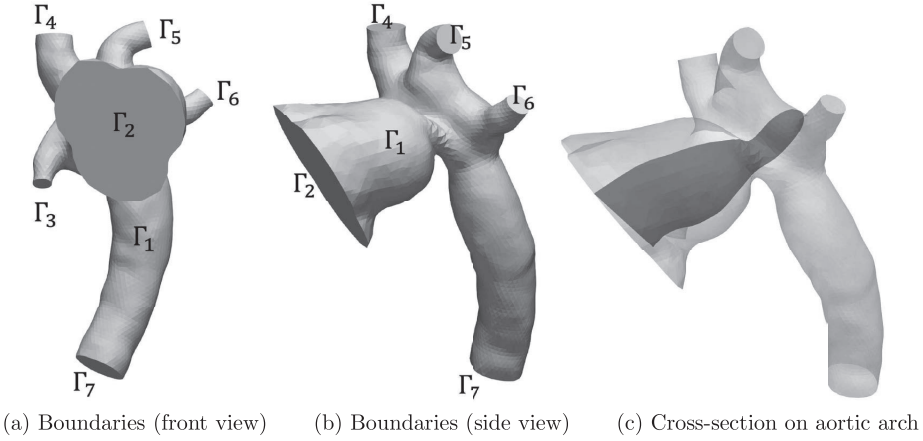
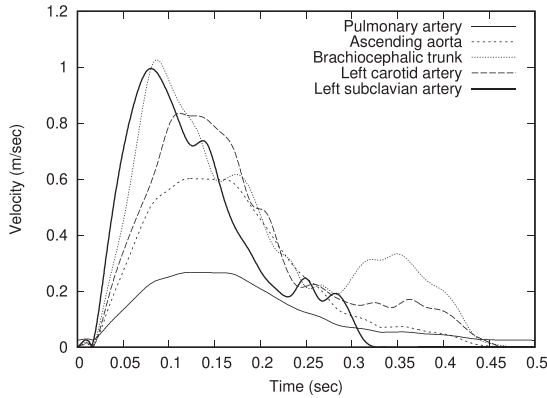Figure 1: Target region configuration.

Figure 2: Velocity profiles.

The anastomosis site forms a thin slit between the pulmonary artery and aortic arch. Figure 3 shows velocity magnitudes on a cross-section where the flows through the slit are apparent. The cross-section location is presented in Fig. 1(c). In Fig. 3, it is apparent that counterclockwise circulation is induced in the aortic arch at the systolic phase.
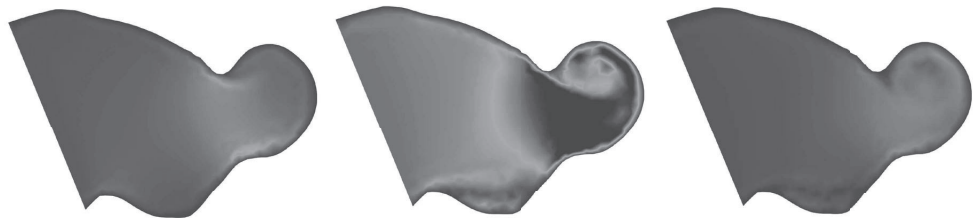
(a) Early systolic phase ($t = 0.04$)   (b) Peak systolic phase ($t = 0.15$)   (c) Late systolic phase ($t = 0.3$)

Figure 3: Velocity magnitudes on a cross-section at the aortic arch.

Then, the circulation in the aortic arch is visualized more closely by drawing instantaneous streamlines at the peak systolic phase in Fig. 4, which shows that the circulation induced by the thin slit at the anastomosis site is distributed widely along the aortic arch and that it flows down to the descending aorta.
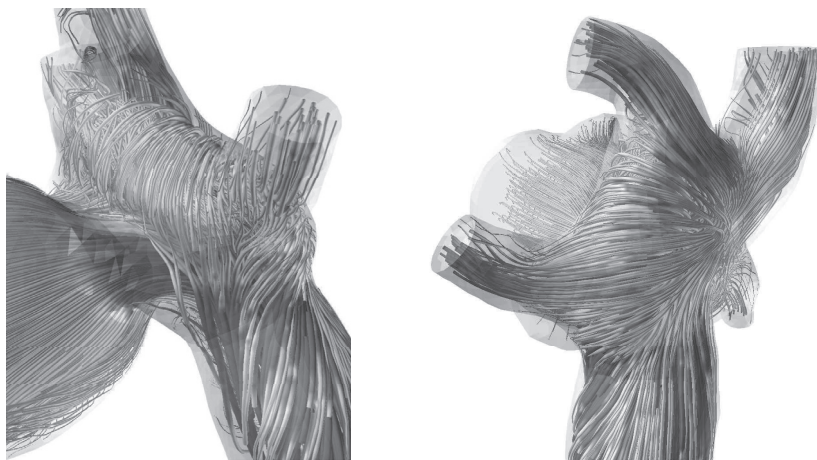

Figure 4: Front and back views of instantaneous streamlines at the aortic arch

Figure 5 portrays the instantaneous streamlines and energy dissipation function defined as

$$\Psi = 2\mu \left(e_{ij} - \frac{1}{3} e_{kk} \delta_{ij} \right)^2,$$ (3)

where e_{ij} is the rate of strain tensor at the peak systolic phase.

From a clinical perspective, energy dissipation distribution is an important quantity because it imposes a load on the heart directly. In Fig. 5(b), high energy dissipation is apparent at the anastomosis site, which can be understood straightforwardly because the velocity is very high there. Although high energy dissipation is also apparent in the descending aorta, it cannot be understood straightforwardly. This dissipation apparently derives from spiral flow there, which is generated at the aortic arch immediately after blood passes out of the thin anastomosis channel as depicted in Fig. 4. Here, a relation can be found between geometrical characteristics and energy dissipation patterns through flow structures.

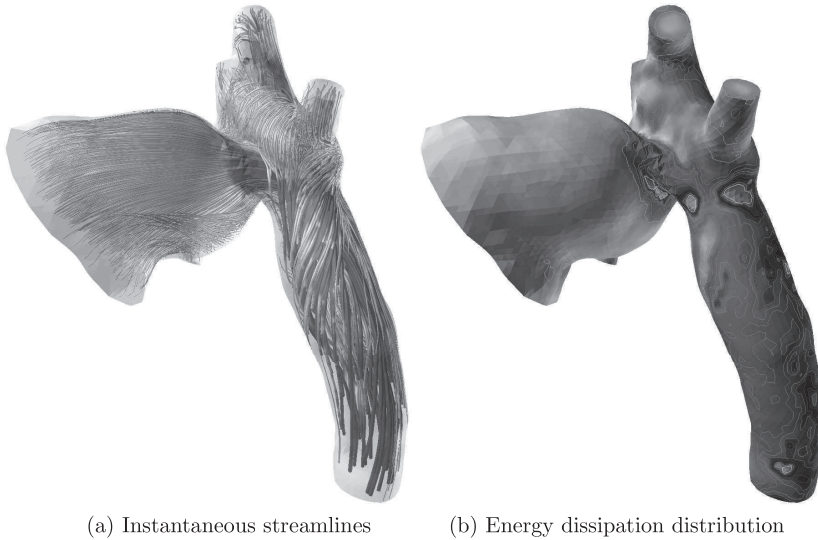(a) Instantaneous streamlines   (b) Energy dissipation distribution

Figure 5: Streamlines and energy dissipation in the aortic arch and the descending aorta.

4   Conclusions

We presented an example of a computational approach to elucidate the relation between geometrical characteristics and flow structures in hypoplastic left heart syndrome. For broader difficulties of clinical medicine, such as clinically meaningful classification of disease states and decision-making support for treatment strategies, pose several mathematical issues. Through close collaboration between mathematical science and clinical medicine, these analyses can be expected to yield greater understanding leading to better risk assessment.

Acknowledgment

References

[1] S.A. Berger, L. Talbot, L.-S. Yao, Flow in Curved Pipes, *Ann. Rev. Fluid Mech.,* 15, 461–512, (1983).

[2] M. Germano, On the effect of torsion on a helical pipe flow, *J. Fluid Mech.,* 125, 1–8 (1982).

[3] T.E. Tezduyar, Stabilized finite element formulations for incompressible flow computations, *Advances in Applied Mechanics,* 28, 1–44, (1992).

[4] J. Jeong and F. Hussain, On the identification of a vortex. *J. Fluid Mech.,* 285, 69–94 (1995).

[5] K.E. Lee, K.H. Parker, C.G. Caro, and S.J. Sherwin, The spectral/hp element modeling of steady flow in non-planar double bends, *Int. J. Num. Meth. Fluids,* 57, 519–529 (2008).

[6] H. Suito, T. Ueda and D. Sze, Numerical simulation of blood flow in the thoracic aorta using a centerline-fitted finite difference approach, *Jpn. J. Ind. Appl. Math.,* 30 (3), 701–710, (2013).

[7] H. Suito, K. Takizawa, V.Q.H. Huynh, D. Sze and T. Ueda, FSI analysis of the blood flow and geometrical characteristics in the thoracic aorta, *Comput. Mech.,* 54 (4), 1035–1045, (2014).

[8] T. Ueda, H. Suito, H. Ota and K. Takase, Computational fluid dynamics modeling in aortic diseases, *Cardiovascular Imaging Asia,* 2 (2), 58–64, (2018).

[9] S. Asada, M. Yamagishi, K. Itatani, Y. Maeda, S. Taniguchi, S. Fujita, H. Hongu, H. Yaku, Early outcomes and computational fluid dynamic analyses of chimney reconstruction in the Norwood procedure. Interact. *Cardiovasc. Thorac. Surg.,* Mar 15, pii: ivz040, (2019).

[10] S. Fujita, M. Yamagishi, Y. Maeda, K. Itatani, S. Asada, H. Hongu, E. Yamashita, Y. Takayanagi, H. Nakatsuji, H. Yaku, The effect of a valved small conduit on systemic ventricle-pulmonary artery shunt in the Norwood-type palliation, *Eur. J. Cardiothorac. Surg,* Jan 2, pii: ezz3779 (2020).